

Antimicrobial Studies of Black Silicon and Black Diamond Using Gram-Positive Bacteria

Neda Norouzi, Willem Woudstra, Edmund J.W. Smith, Gulnur Zulpukarova, Kaili Yao, Viraj G. Damle, Romana Schirhagl,* Paul W. May,* and Tom Kamp

Herein, it is investigated if black diamond is useful in a bactericidal surface. Black diamond is derived from black silicon, a silicon surface structured into nanosized needles. Black diamond is obtained by coating black silicon with a thin diamond film, rendering the nanostructures more robust. The bactericidal and antibacterial properties of fluorine-terminated and hydrogen-terminated black diamonds with those of black silicon and for flat surfaces of diamond (on silicon) with the same terminations are studied. The ability to repel and kill Gram-positive *Staphylococcus aureus* and *Staphylococcus epidermidis* is evaluated, which have a thicker cell wall and are more mechanically robust than the bacteria that are studied before. The initial adhesion as well as long-term 24 h biofilm formation is studied. The number of bacteria that initially adhere to the fluorine-terminated black diamond surface is reduced and has the highest dead bacterial ratio. Biofilm formation after 24 h shows that while all surfaces outperform glass over the long term, diamond-coated surfaces with both fluorine and hydrogen termination have a significant inhibiting biofilm formation effect. In conclusion, fluorinated and hydrogenated diamond-coated surfaces with and without nanoneedles have repelling, bactericidal, and biofilm-inhibiting effects on Gram-positive bacterial strains and are promising antimicrobial surfaces.

1. Introduction

With the rise in antibiotic-resistant bacteria also comes a high demand for antibacterial, antifouling, and bactericidal materials that are not based on antibiotics. Many such materials have been developed in recent years, including particle-based systems^[1–4] and surfaces that repel or kill bacteria on contact.^[5–8] An interesting class of antibacterial surfaces are nanostructured surfaces which act in two main ways,^[9] sharp structures that can pierce the bacterial cell wall^[10–12] and mechanical stress causing the cell wall to rupture as bacteria are stretched on the surfaces.^[13] One such material is black silicon, a synthetic nanostructured material with high-aspect-ratio nanoprotusions, such as nanospikes or nanoneedles, on its surface produced through plasma etching.^[14] The name “black silicon” originates from its deep black color, resulting from the absorption of >99% of the visible light falling onto its surface. It has now found applications

in photovoltaics^{15,16} and has recently been used for biomedical sensing applications.^[17,18] Black silicon has an excellent bactericidal effect that can be tuned by varying the lengths and spacing of the nanoscale needles.^[19] However, silicon nanoneedles are relatively fragile^[20] and thus, it would be desirable to improve their mechanical properties and durability. The aim of this article was to improve the mechanical stability of black silicon while retaining or even improving the antibacterial properties. To this end, the black silicon (bSi) needles were conformally coated with a thin (<500 nm) layer of diamond using a chemical vapor deposition (CVD) process. This new composite material has been labeled ‘black diamond’ (bD),^[21] and it has been shown previously that these bD surfaces retain many of the bactericidal properties of bSi while being chemically more inert and mechanically more robust.^[19,20,22]

Previous work of this type has been performed mostly using Gram-negative bacteria.^[20,21] While in some cases, Gram-positive and Gram-negative bacteria behave in a similar fashion, this is not necessarily the case.^[23,24] On some surfaces, Gram-positive and Gram-negative bacteria behave totally differently depending on the surface characteristics.^[25,26] Thus, it is crucial to investigate both types of bacteria to have a complete picture of the bactericidal properties of a surface.

N. Norouzi, W. Woudstra, V. G. Damle, R. Schirhagl
Department of Biomedical Engineering
UMCG
Antonius Deusinglaan 1, 9713 AV Groningen, The Netherlands
E-mail: romana.schirhagl@gmail.com

E. J. W. Smith, G. Zulpukarova, K. Yao, P. W. May
School of Chemistry
University of Bristol
Bristol BS8 1TS, UK
E-mail: paul.may@bristol.ac.uk

T. Kamp
Lam Research
4400 Cushing Parkway, Fremont, CA 94538, USA

 The ORCID identification number(s) for the author(s) of this article can be found under <https://doi.org/10.1002/adem.202301031>.

© 2023 The Authors. Advanced Engineering Materials published by Wiley-VCH GmbH. This is an open access article under the terms of the Creative Commons Attribution License, which permits use, distribution and reproduction in any medium, provided the original work is properly cited.

DOI: 10.1002/adem.202301031

For the experiments in this article, two types of Gram-positive bacteria were chosen which are currently the most common causative strains for biomaterial-associated infections: *Staphylococcus aureus* (*S. aureus*) and *Staphylococcus epidermidis* (*S. epidermidis*).^[27] One important difference between these two bacterial strains is their extracellular polymeric substance (EPS) excretion ability.^[28]

S. aureus is a Gram-positive, spherical-shaped, nonmotile bacterium with high EPS excretion ability and is frequently found in the upper respiratory tract and on the skin. It is an opportunistic pathogen and a common cause of skin infections, respiratory infections, and food poisoning.^[29] Some *S. aureus* infections can be treated with antibiotics such as penicillin and vancomycin. However, recent antibiotic-resistant strains, such as methicillin-resistant *S. aureus* (MRSA), are now proving problematic to treat, leading to many deaths.^[30]

S. epidermidis is also a Gram-positive, spherical-shaped, nonmotile bacterium found as part of the commensal skin flora.^[31] However, it has low or no EPS excretion ability compared to *S. aureus*. *S. epidermidis* is not usually pathogenic; however, patients with compromised immune systems can be at risk of developing hospital-acquired infections. It is also a frequent contaminant of laboratory specimens and medical equipment, such as catheters. *S. epidermidis* strains are often resistant to antibiotics. However, their ability to form biofilms on plastic devices is a major problem because other bacteria can bind to them, creating a multilayer and multispecies biofilm with increased antibiotic resistance.^[32]

2. Experimental Section

2.1. Black Silicon and Black Diamond Samples

Black silicon wafers were supplied by LAM Technologies in the form of 12 inch Si wafers. They were manufactured from blank Si wafers in a Lam KyoGX TCP reactive-ion etcher using an SF₆/O₂ process gas mixture. Radio-frequency power was inductively coupled into the gas mixture via a transformer to create a plasma and control the ion density, while ion bombardment onto the wafer was regulated via a separate applied platen bias. This process was optimized to oxidize and etch the Si simultaneously, producing micromasks that enabled the Si to be etched anisotropically into nanosharp spikes or needles. The morphology of the needles and the flat surfaces was determined by scanning electron microscopy (SEM). In order to prepare samples for SEM, they were sputter coated with Ag using an Agar high-resolution sputter coater and a target of Ag of 99.99% purity. Samples were coated between 15 and 20 nm. The micrographs were recorded in secondary-electron detection and backscattered electron detection mode, respectively.

These needles were 5–10 μm long, with tip separation of 0.25–0.5 μm, as verified by SEM (JSM-IT300, 15 kV) in **Figure 1a**) and a tip radius of ≈20 nm, verified previously by transmission electron microscopy (TEM). Chemical characterization of the samples was also done previously by Raman spectroscopy.^[20]

These wafers were mechanically cleaved into smaller-sized pieces for experimental use, with some receiving subsequent diamond coating. Samples to be diamond coated were seeded

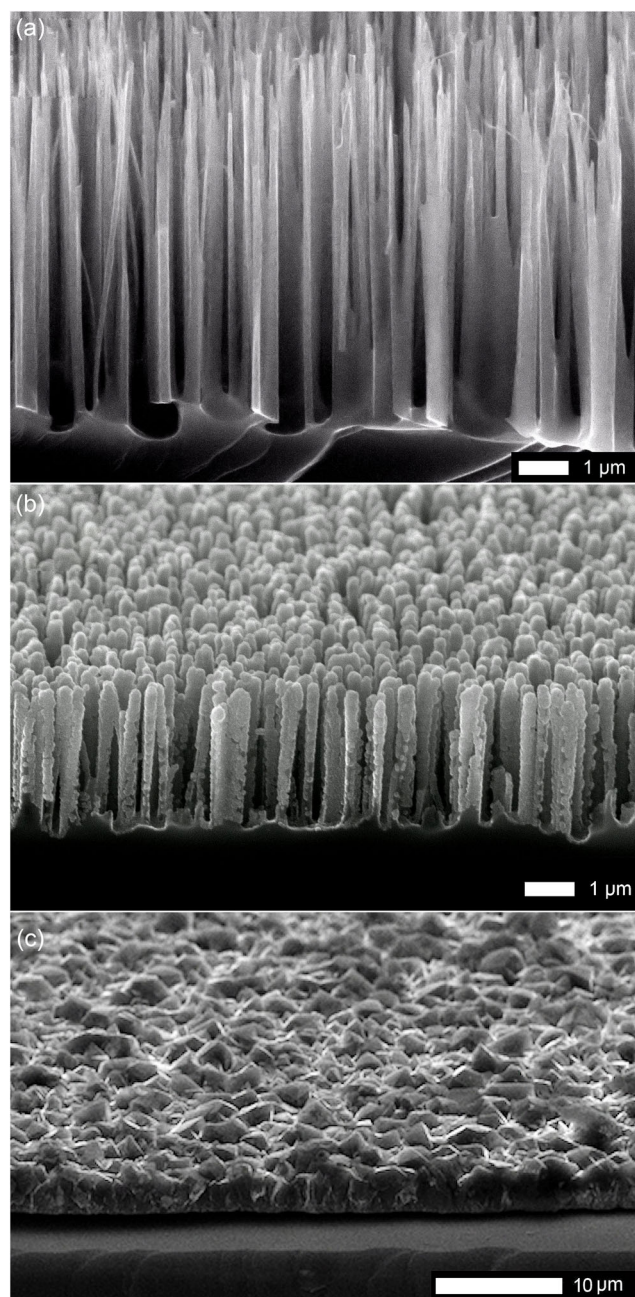


Figure 1. SEM micrographs of a) a cross section through a bSi wafer, b) a representative sample of a bD wafer, and c) a 'flat' diamond control wafer (i.e., a uniform, pinhole-free microcrystalline diamond film on a Si substrate).

with 4–10 nm detonation nanodiamond (DND) using a suspension of DND in methanol into which the samples were submerged for 1 h and then gently blown dry. This method allowed a near monolayer of diamond seeds to coat the entire surface of the needles without causing any damage and was necessary to ensure subsequent diamond growth occurred uniformly over the entire surface. The seeded samples were then placed into a hot-filament CVD diamond reactor, and a thin

(<100 nm) film of undoped microcrystalline diamond was deposited conformally onto the needles using standard CVD conditions (20 torr, 1% CH₄/H₂) for 30 min. The diamond deposition was optimized for these structures with the main criteria that Si needles should be completely coated in diamond, leaving no Si exposed, even down to the base of the needle.^[33] This required dense seeding with nanodiamond particles to form almost a monolayer coverage, before CVD began, and the seeds were grown into a continuous conformal coating. The CVD chamber could accommodate 2 samples; therefore, this seeding and deposition process was repeated several times to provide multiple identical samples to ensure statistical reliability. Over the time taken to grow the multiple samples required, SEM images were taken at regular intervals to ensure that the coatings were identical across the sample set.

Example SEM images of the diamond-coated bSi samples (hereafter referred to as black diamond) are shown in Figure 1b. It is clear that the diamond CVD process etched away the needles such that they were now around 3–4 μm long, but the diamond coated them uniformly and conformally down to the base. The tips became rounded, with a tip radius of ≈100 nm, although the tip-to-tip separation remained ≈0.25–0.5 μm. For further details, we refer to Dunseath et al.^[22]

As deposited, these bD samples were all hydrogen terminated as a result of the CVD process, meaning they were slightly hydrophobic.

2.2. Flat Control Samples

Samples consisting of CVD diamond grown onto flat Si substrates were also prepared to act as control samples. Undoped Si (100) substrates were mechanically cleaved into smaller pieces and subsequently mechanically abraded using 1–3 μm diamond powder and then placed into the hot filament CVD reactor using the same conditions as before, except for 8 h. This allowed a continuous microcrystalline diamond film to be deposited of thickness ≈3 μm. As Figure 1c shows, these samples are not absolutely flat but consist of randomly oriented faceted diamond crystallites and surface topography with an average roughness ≈0.25 μm. The crystallites here were of the order of ≈1 μm, and the root mean square (RMS) roughness was similar, at ≈1 μm (see Table S1, Supporting Information). Other control samples used for microbiological testing were glass and uncoated bSi wafers.

2.3. Fluorine Termination

Half of the flat control, bSi and bD sample surfaces were fluorinated by exposing them to SF₆ plasma for 10 s in a home-built DC plasma reactor. This process replaced the C–H bonds on the exposed surfaces with C–F bonds, making the surfaces very hydrophobic. SEM images were taken, as described above, to ensure that this fluorination process did not affect the surface morphology in any visible manner (see Figure S1, Supporting Information). Water droplet tests showed that the F-termination behaved as expected, the water contact angle (WCA) significantly increased on the bD surface from 108° (H-terminated) to 141° (F-terminated), showing a large increase in the hydrophobicity. For the “flat” diamond control samples, there was only a very

small change in the WCA from 84° to 98° after F termination (see Table S1, Supporting Information), mostly because the much smoother surface made the water spread more readily. These values were consistent with results from previous experiments.^[22] Chemical characterization of the samples via X-ray photoelectron spectroscopy (XPS) was performed previously.^[22]

2.4. Bacterial Culture Conditions

Frozen (–80 °C) bacterial stocks in 7% DMSO of *S. aureus* ATCC 12600 and *S. epidermidis* ATCC 12228 were streaked onto a blood agar plate (5% sheep blood) and incubated for 24 h at 37 °C aerobically. After incubation, a single colony was transferred into a preculture of 10 mL tryptone soya broth (TSB), vortexed, and incubated at 37 °C for 24 h aerobically. Main cultures were prepared by transferring 2 mL of the preculture into 40 mL TSB and incubating for 16 h aerobically. Bacterial suspensions were then diluted into TSB in a 1:20 volume ratio and further incubated at 37 °C for 4 h aerobically until the midexponential phase was reached. Bacterial cells were then washed twice in 10 mM Tris-HCl buffer and harvested by centrifuging at 5000 g at 10 °C followed by sonication for 3 × 10 s at 30 W (Sonics and Materials Inc. Newtown Connecticut USA, Vibra cell VXC 130) to break apart bacterial aggregates.^[20,34] The cells were then enumerated using a Bürker-Türk counting chamber.

2.5. Bacterial Growth

To prepare the surfaces for testing of their bactericidal activity, all surfaces were first rinsed with ethanol 70% to disinfect them. Then the samples were placed into 12-well plates, to which 2 mL of bacterial suspension of 1 × 10⁷ of *S. aureus* ATCC 12600 or *S. epidermidis* ATCC 12228 per mL were added, depending on the experimental group. These samples were incubated for short term (1 h) or long term (24 h) aerobically at 37 °C under static conditions. Surfaces were then rinsed by gently washing five times in Tris-HCl buffer in a universal container without damaging the surface before testing the bactericidal properties.^[20]

2.6. Testing Bactericidal Properties

To evaluate the surfaces for their short-term bactericidal activity and study the initial bacterial adhesion, Live/Dead BacLight (Bacterial Viability Kit, for microscopy & quantitative assays, Thermofisher) bacterial viability stain was added to the surfaces that were incubated with bacteria for 1 h in Tris-HCl buffer. Once stained, the samples were left in the dark for 15 mins at room temperature. After staining, the samples were transferred to a new 12-well plate containing phosphate buffer saline (PBS). Bacterial cell viability was visualized by fluorescence microscopy (Leica Microsystems CMS GmbH, Type DM4000B, Camera: Leica DFC350, 40× water immersion objective). In three independent experiments, five images of each surface were taken each time. Numbers of live (stained with SYTO9, green) and dead (stained with propidium iodide (PI), red) bacterial cells were quantified by manually counting using *ImageJ* software version 1.53c with the cell-counter plugin.^[35]

To evaluate the surfaces for their long-term bactericidal activity, the viability of the bacterial biofilm was quantified. First, all studied surfaces were inoculated with bacterial suspension in TSB and incubated at 37 °C under static conditions for 24 h. After incubation, the surfaces were washed twice with PBS. Next, the biofilms were stained for 15 min with Live/Dead BacLight bacterial viability stain as described previously. Finally, confocal laser scanning microscopy (CLSM) was applied to observe a biofilm structure using a Leica Stellaris 5 (LAS X software version 4.3) with a DM6 upright microscope (Leica Microsystems CMS GmbH). The excitation and emission were set at 488/500 nm for SYTO9 and 561/635 nm for PI. 2% laser power, pinhole of 1, and a 40× water immersion objective were used to observe the biofilm. Image stacks were recorded with an *xy* resolution of 1024 × 1024 pixels (292 × 292 μm) and *z*-stack images were taken in 1 or 2 μm steps, depending on the biofilm thickness. To quantify bacterial biofilm, the biofilm structural parameters, including biomass and average thickness, were calculated using COMSTAT 2.1 software from nine biofilm image stacks of each surface from three independent experiments.^[36,37]

To assess the biofilm formation, the samples that were incubated for 24 h were imaged using an optical coherence tomography (OCT) Ganymede II (Thorlabs Ganymede, Newton, NJ, USA) with a 930 nm center wavelength white-light beam and a Thorlabs LSM03 objective scan lens, able to provide a maximum scan area of 100 mm². The imaging frequency was 30 kHz with a sensitivity of 101 dB and the refractive index of biofilms was set as 1.33, equal to that of water. 2D images were fixed at 5000 pixels but with variable pixel sizes depending on magnification in the horizontal direction while containing a variable number of pixels with 2.68 μm pixel size in the vertical direction. Images were created by the OCT software (ThorImage OCT 5.4.7.0). Three independent experiments each containing four biofilm images of each surface were used to analyze the biofilm height using in-house developed software (LabVIEW 2018, Version 18.0, National Instruments).^[38]

2.7. Testing Surface Morphology after Bacterial Adhesion

SEM was performed to visualize morphological details on the bacteria–surface interface. Sample preparation was done as described by Hazell et al.^[20] Briefly, the bacteria were fixed onto the surface by immersion in a 2.5% glutaraldehyde solution in 0.1 M potassium phosphate buffer for 2 h at room temperature. The surfaces were then dehydrated by sequential immersion in 20%, 40%, 60%, 80%, and 100% ethanol for 10 min each and finally hexamethyldisilazane for 10 min. Before SEM imaging, dried sample stages were sputtered with a 30 nm gold layer and a Philips XL30 instrument was used to record the images at 10 kV.

2.8. Statistical Analysis

Statistical analysis was performed with GraphPad Prism version 8 (GraphPad Software, La Jolla California USA). An unpaired *t*-test was used for analysis between two groups, and for three groups or more a One-Way ANOVA test with a Tukey post hoc test was performed. A statistical difference was indicated with an asterisk, **p* < 0.05, ***p* < 0.01, ****p* < 0.001, *****p* < 0.0001.

We performed a normality test “Shapiro-Wilk”. Most conditions conformed to the normal distribution. There were a few conditions that did not meet the standards of the normality test; however, being biological samples, they were sampled from an assumed normal population, making the ANOVA an acceptable test to maintain statistical power.

3. Results and Discussion

3.1. Short-Term Adhesion

The irreversible attachment of bacteria to materials is a pivotal step toward establishing a biomaterial-associated infection. In general, nanostructured surfaces have shown reduced bacterial adhesion due to the fact that nanostructuring decreases the contact area between the surface and adhering bacteria.^[39] To this end, we tested whether our surfaces were able to prevent bacteria from initial adhesion or kill them in the short term by staining live and dead bacteria after 1 h. Live bacteria with an intact membrane stained green while compromised membranes showed red, which are considered dying or dead. **Figure 2a** shows representative fluorescence micrographs of *S. aureus* on different surfaces after conducting the live-and-dead assay. **Figure 2b** shows a quantitative analysis of adhered *S. aureus* after the short-term adhesion of 1 h. Comparing the different surfaces, both F- and H-terminated Flat and bSi surfaces had the most bacteria attached, which was similar to the value for glass. In contrast, both F- and H-terminated bD surfaces were able to repel *S. aureus* more than their flat counterparts and the bSi surface. A remarkable observation is the 50% dead bacteria and significant difference (*p* < 0000.1) for the F-terminated bD surfaces in adhered bacteria compared to the other surfaces. While on F- and H-terminated diamond-coated nanostructured surfaces, 50% and 25% of the attached bacteria were killed respectively, only between 4% and 15% of the *S. aureus* were killed on the F- and H-terminated flat and bSi surfaces. This was determined by counting cells in confocal images after live–dead staining.

The bacterial adhesion after 1 h for *S. epidermidis* was imaged by fluorescence microscopy and shown in **Figure 3a** while the quantification of the adhered bacteria is represented in **Figure 3b**. The most remarkable observation was the significantly reduced bacterial adhesion on the F-bD surface compared to other surfaces. *S. epidermidis* adhered best to the F- and H-terminated flat surfaces, in similar bacterial numbers to those for *S. aureus*. It is worth mentioning that for *S. epidermidis*, fewer dead bacteria were observed compared to *S. aureus* on all surfaces except for F-bD. The reduced number of dead bacteria could be explained by the ability of *S. aureus* to excrete EPS.^[26] *S. aureus* is a high-level EPS producing strain,^[27] leading to stronger attachment to surfaces. In contrast, *S. epidermidis* produces less EPS and likely attaches more loosely to the surface.^[27] As a result, *S. aureus* might be more vulnerable to being pierced mechanically by surface structures or affected by surface chemistry, resulting in increased dead *S. aureus* bacteria compared to *S. epidermidis*. While the size of bacteria and thus the number of needles that could potentially pierce the bacterial cell wall were reported before to influence the death rate,^[20,22] this is unlikely to be the reason for the differences here, because both bacteria are very similar in size.

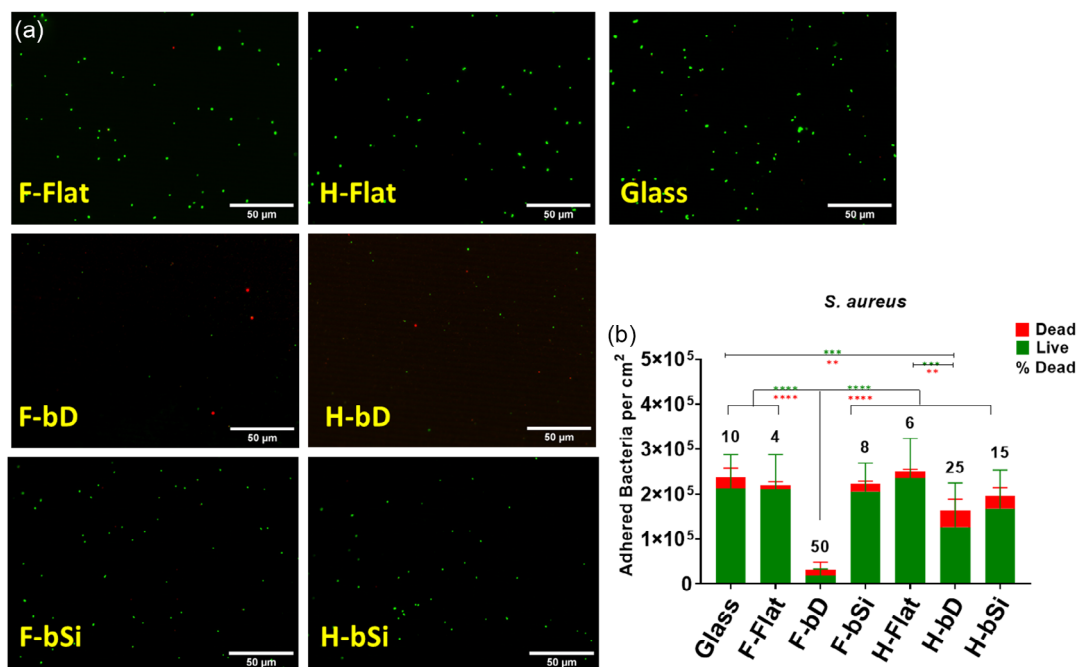


Figure 2. Adhesion of *S. aureus* after 1 h on flat, bD, and bSi surfaces with F- and H-termination. a) Representative live/dead fluorescent images of the different surfaces after 1 h adhesion of *S. aureus*. b) The quantitative analysis of bacterial adhesion and live/dead assay (red represents dead cells stained by PI and green represents living cells stained by SYTO9). The percentage of dead cells is shown on top of each column. Error bars represent the standard deviation of three independent experiments (with five images each). Asterisks indicate a significant difference: green font are for comparing live bacteria cells and red font are for comparing dead bacteria cells as a percentage.

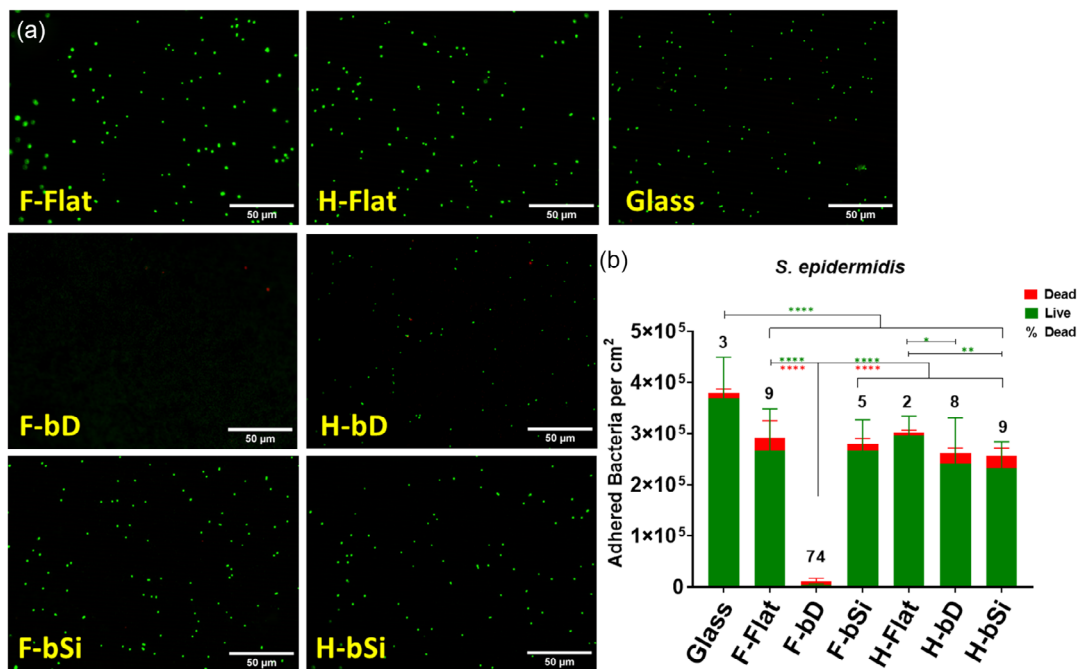


Figure 3. Adhesion of *S. epidermidis* after 1 h on Flat, bD, and bSi surfaces with F- and H-termination. a) Representative live/dead fluorescent images of the different surfaces after 1 h adhesion of *S. epidermidis*. b) The quantitative analysis of bacterial adhesion and live/dead assay (red represents dead cells stained by PI and green represents living cells stained by SYTO9). The percentage of dead cells is shown on top of each column. Error bars represent the standard deviation of three independent experiments (with five images each). Asterisks indicate a significant difference: green font are for a comparison of live bacteria cells while red font are for a comparison of dead bacteria cells as a percentage.

While a reduction in bacterial adhesion in both F- and H-terminated bD samples was observed, F-bD samples showed a significantly increased reduction in bacterial adhesion. Also, for *S. epidermidis*, a higher percentage of dead bacteria was observed on the F-terminated bD, although the effect was less pronounced than that observed for *S. aureus*.

In the literature, there are some reports where bacteria adhere better to hydrophobic surfaces.^[40] Thus, it is surprising that fewer bacteria adhered to the F-terminated surfaces, which have been shown to be hydrophobic.^[16] Comparing to earlier results^[20,22] on Gram-negative (*Escherichia. coli* K12) and Gram-positive (*Streptococcus gordonii* DL1) bacteria, we see much less adhesion of Gram-positive *S. aureus* and *S. epidermidis* bacteria. The two primary trends observed in our results were that fewer bacteria adhered to the F-terminated bD, which also killed more bacteria, which reflect results found by prior work.^[21] We also achieved higher bactericidal efficacy when using F-bD than reported for Gram-negative bacteria on a similar surface.^[20,22]

The possible mechanism for bacterial death is the mechanical stretching of the bacteria across several needles causing the cell wall to rupture, assisted by the piercing of the wall by the needle itself.^[11,41] However, there are also reports in the literature where

bacteria were stretched but not killed, and killing has been attributed to oxidative stress that is formed at the surface.^[42] We do not consider the formation of oxidative stress very likely in this case since nanodiamonds have been shown to be very biocompatible and did not induce oxidative stress in mammalian cells or bacteria in particle form.^[43,44] As was found in prior work, Gram-negative bacteria are often easier to kill through this mechanism, mostly because the bacterial cell walls are less rigid and hence stretch on the needles more easily as the bacterium moves.^[19] However, we show here that with needles of the correct size (3–4 μm), distribution (0.25–0.5 μm), surface hydrophobicity ($\approx 140^\circ$), termination (fluorinated), and diamond coating (4–10 nm), Gram-positive bacteria are equally, if not more, susceptible to this mechanism of bacterial death, as the bacterial walls of these nonmotile bacteria are more rigid and as a consequence will rupture with less stretching.^[9]

While Gram-negative bacteria are more prone to developing antibiotic resistance and are considered harder to treat, Gram-positive bacteria are, for instance, more resistant to irradiation.^[45] Thus, it is not obvious that they are also vulnerable to being pierced mechanically or being ruptured due to being stretched.

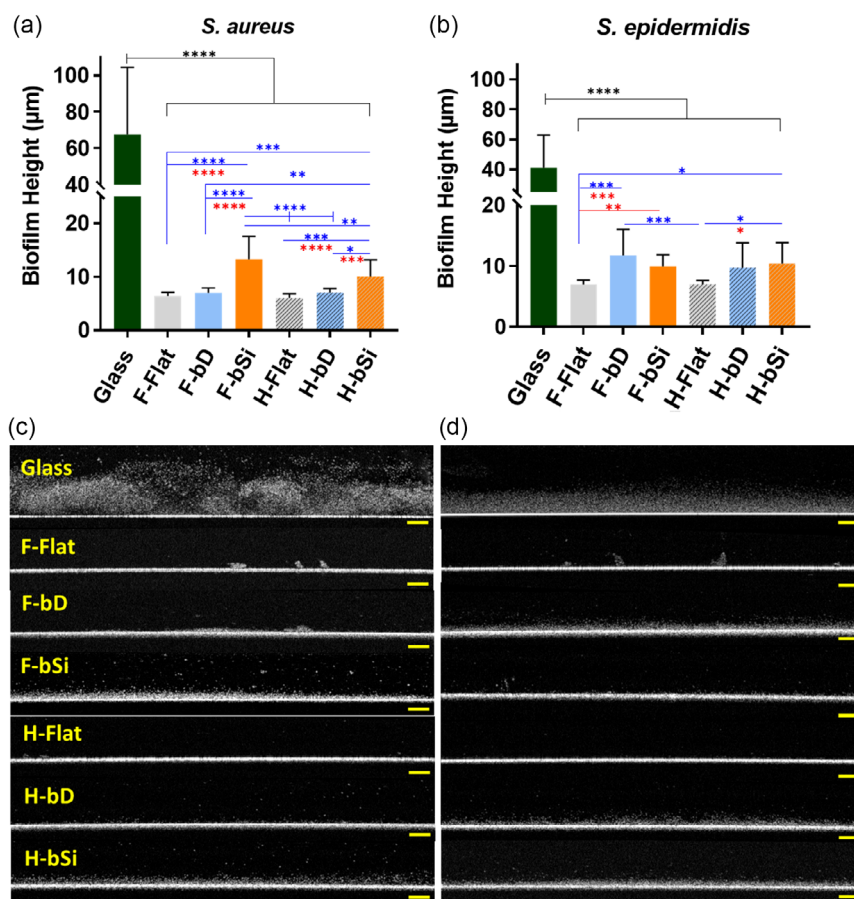


Figure 4. Evaluation of the long-term 24 h biofilm formation on different surfaces analyzed by OCT. A quantitative analysis of a) *S. aureus* and b) *S. epidermidis* biofilm height. Error bars represent the standard deviation of three independent experiments of four separate images. Asterisks indicate a significance difference. Black* glass versus all tested surfaces, blue font each tested surface versus the others, and red font each tested surface versus two other surfaces in the same group. Representative OCT images of the resulting 24 h c) *S. aureus* and d) *S. epidermidis* biofilms on the different surfaces. Scale bars indicate 100 μm .

3.2. Long-Term Biofilm Formation

After comparing the 1 h short-term prevention of bacterial adhesion on the different surfaces, long-term biofilm formation of *S. aureus* and *S. epidermidis* after 24 h was evaluated, with the biofilm height results and micrographs of the OCT shown in Figure 4.

The initial short-term bacterial adhesion showed promising repelling and contact-killing properties, especially for the F-bD surface (Figure 2b and 3b), but eventually after 24 h bacteria grew on all the surfaces (Figure 4c,d). Nevertheless, all surfaces showed significant biofilm-inhibiting properties compared to the glass control for both *S. aureus* and *S. epidermidis*. Furthermore, the diamond-coated flat and bD surfaces show even better biofilm-inhibiting properties compared to bSi alone, which is more evident in *S. aureus* (Figure 4a). Surprisingly, the bD surfaces eventually showed more bacterial growth than their flat counterparts (Figure 4a,b), which might be explained by the more readily available DNDs on flat surfaces compared to bD. In our previous work regarding DNDs, we proposed a model where DNDs are inhibiting proliferation and facilitating cluster

forming and thus inhibiting biofilm formation. On the other hand, similar behavior was also observed by Li et al. who also observed (for different materials and different bacteria) that the most promising materials in short-term experiments were not the same materials that performed best in long-term experiments.^[46] Also similar findings were reported by Gupta et al.^[47] who observed *S. aureus* adhesion to different materials. Although only short adhesion times below 15 mins were observed, they found that some materials attracted more bacteria early in the experiment but became slower to attract subsequent bacteria.

As in all biological environments, macromolecules such as proteins adsorb onto a surface, which results in a conditioning film for subsequent bacteria adhesion. This can occur on any hydrophobic or hydrophilic surface within minutes.^[48] The conditioning film is able to change the initial surface physicochemical properties (e.g., surface charge, contact angle, chemical composition, and roughness) and thereby the antimicrobial properties.^[48] It has been reported that conditioning films can decrease or increase the hydrophobicity depending on nutrient composition,^[49] which might also be the case for our surfaces

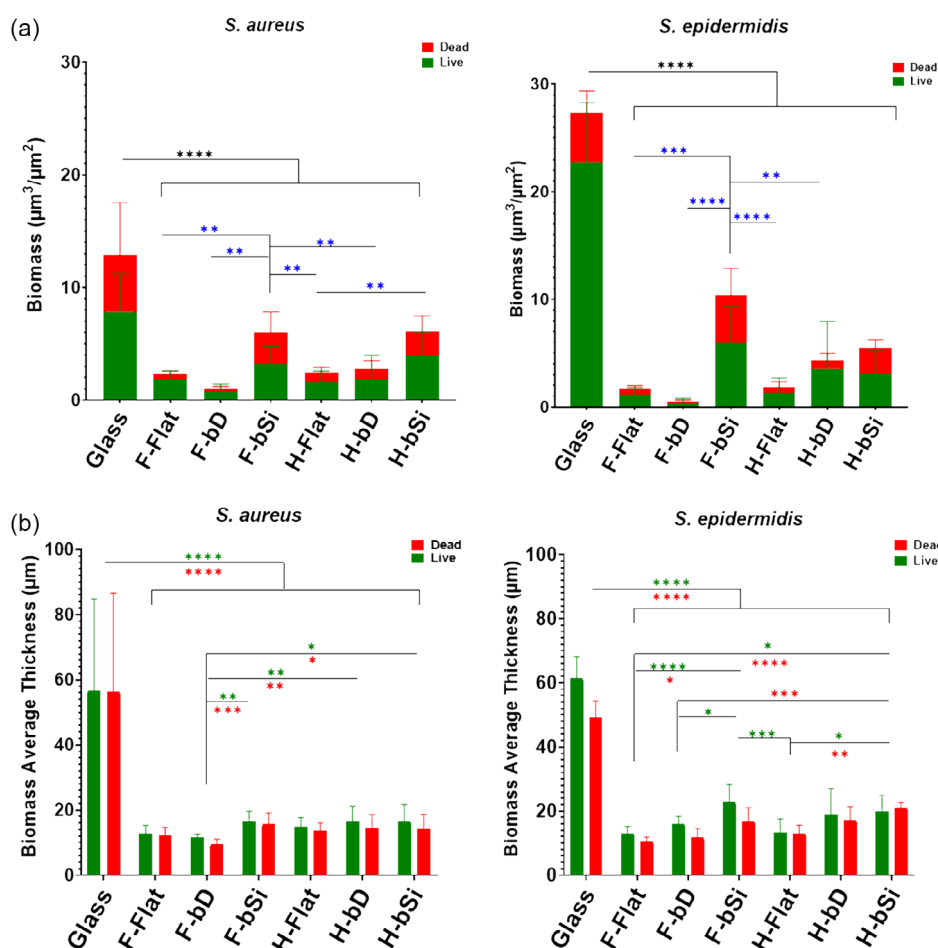


Figure 5. Evaluation of long-term 24 h biofilm formation on different surfaces analyzed by CLSM. A quantitative analysis of a) *S. aureus* and b) *S. epidermidis* biomass. Error bars represent the standard deviation of three independent experiments of three separate z-stacks. Asterisks indicate a significant difference, black* glass versus all tested surfaces, blue font each tested surface versus the others, green font comparison of live bacteria, and red font comparison of dead bacteria.

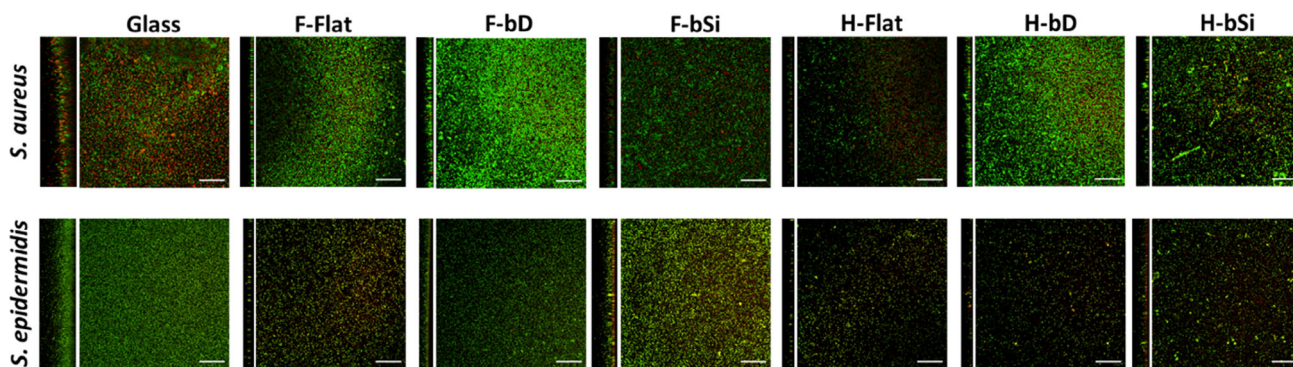


Figure 6. Representative single-slice and side-view micrographs of live and dead bacteria in 24 h biofilms of *S. aureus* or *S. epidermidis* grown on different surfaces imaged by CLSM. Biofilm cells were stained with SYTO9 (green = live) and PI (red = dead) fluorescent dye. Scale bars indicate 50 μm .

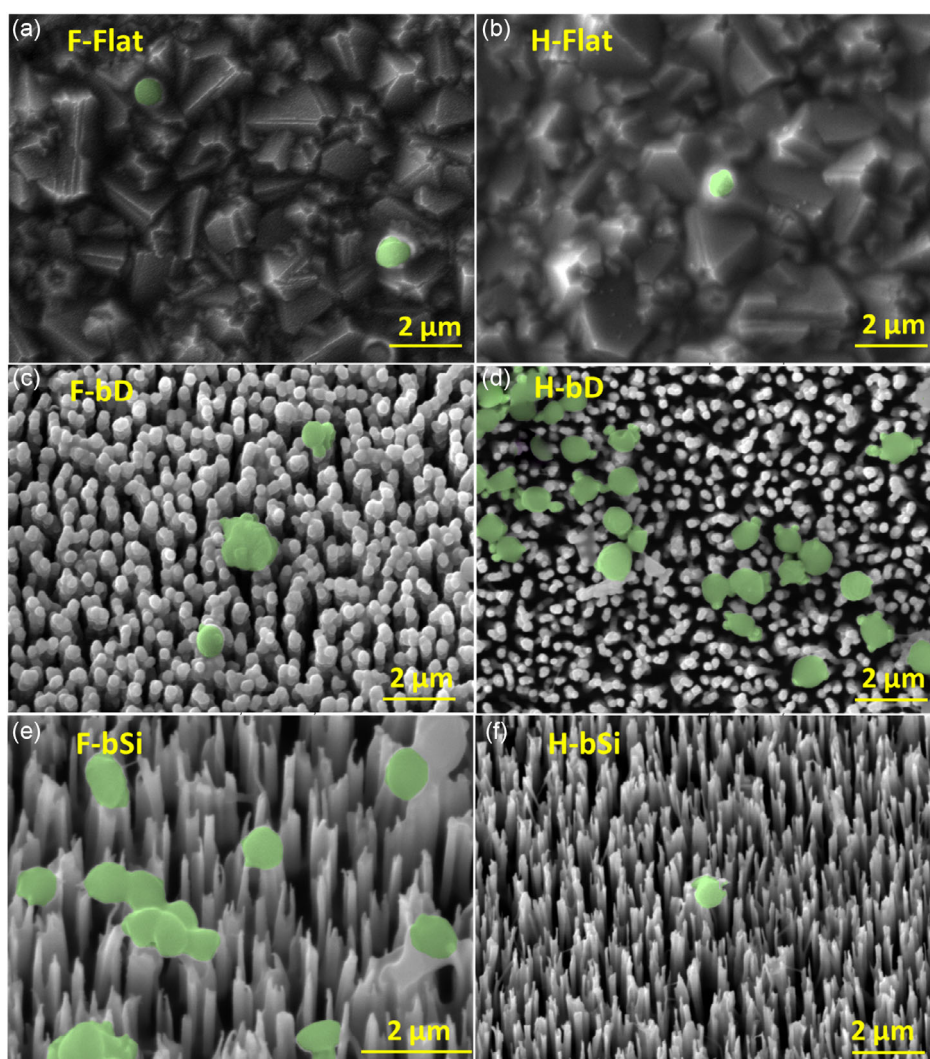


Figure 7. False-color SEM micrographs of the interaction between *S. aureus* (green spheres $\approx 0.5\text{--}1\ \mu\text{m}$ in diameter) and the different surfaces. a) F-terminated flat diamond, b) H-terminated flat diamond, c) F-terminated bD, d) H-terminated bD, e) F-terminated bSi, and f) H-terminated bSi.

and explain why the flat surfaces perform better in the long-term experiments (contact angle is possibly similar before and after conditioning films) compared to the other surfaces.

Another explanation might be the fact that EPS provides viscoelastic properties to a biofilm that are pivotal for its survival against biological, mechanical, and chemical stresses.^[50]

The other possible reason could be that while more bacteria are killed quickly by contact killing, the dead bacteria then remain stuck to the surface; these bacterial remains may provide nutrients to subsequent bacteria, along with a better-suited surface upon which to adhere compared with direct contact with the functionalized spiky surface. This would imply that in order for nanostructured surfaces to be effective in the long-term prevention of bacterial build-up, the dead bacterial remains need to be regularly removed, for example, by frequent washing. It is worth noting that similar nanostructured surfaces in the biological world, such as those found on certain insect wings, would receive frequent washing by exposure to rain.

The biofilm height quantified by OCT was validated with biomass and biomass average thickness by CLSM, as shown in **Figure 5**. Representative CLSM micrographs of the biofilm for *S. aureus* and *S. epidermidis* are shown in **Figure 6** and S2, Supporting Information. The biofilm biomass (Figure 5a) and thickness (Figure 5b) values show a similar trend regarding the

biofilm formation; live and dead bacteria are distributed throughout the whole biofilm (Figure 5b) of diamond coated surfaces.^[51] All surfaces are significantly inhibiting toward biofilm formation compared to glass, although F-bD outperforms the flat surfaces in some cases; both diamond-coated surfaces significantly reduce biofilm formation compared to the bSi alone. These results show the added value of diamond coating alone (i.e., even without nanostructuring) for improved antimicrobial surface properties.^[9,20]

3.3. Investigating the Interaction between Surfaces and Bacteria

As mentioned earlier, previous reports have established that bD and bSi needles kill Gram-negative bacteria by either piercing or rupturing their cell walls.^[9] To determine if that is also the case for Gram-positive *S. epidermidis* and *S. aureus*, the bacterial adhesion was analyzed using SEM (**Figure 7** and **8**). Consistent with the results from fluorescence microscopy

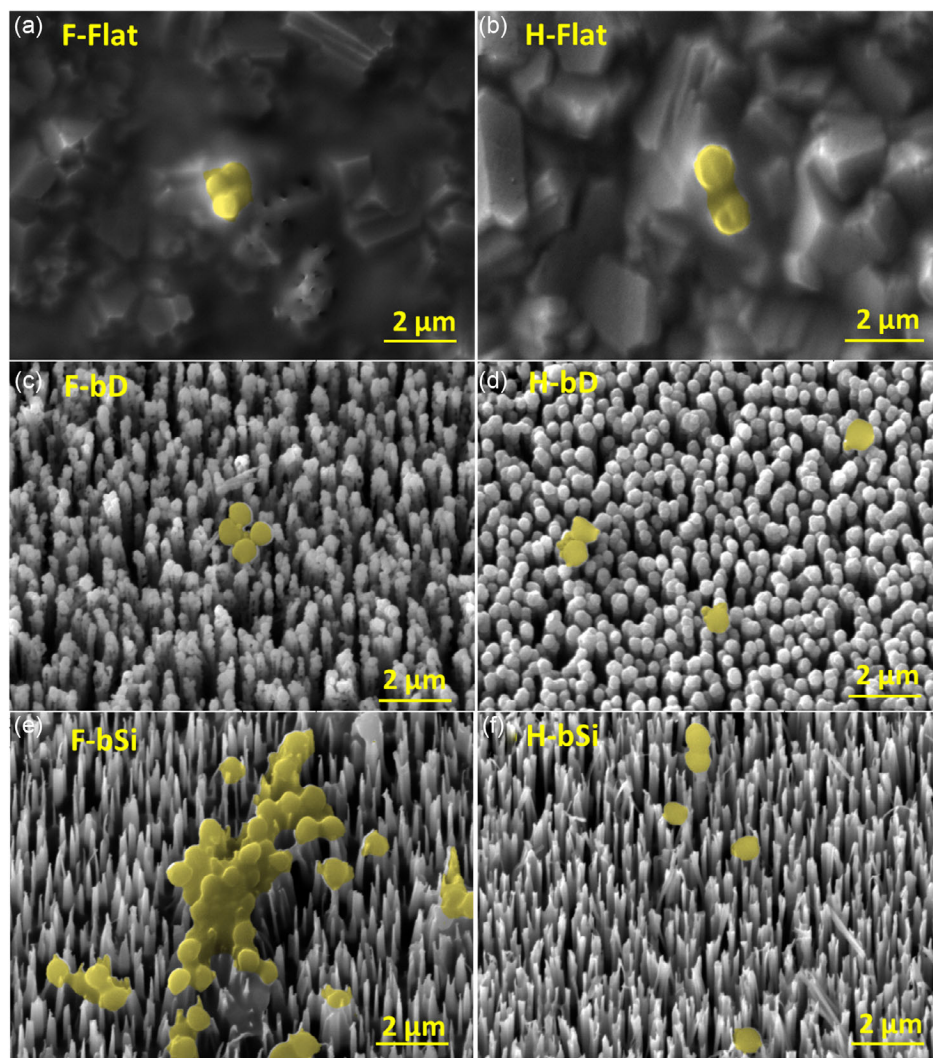


Figure 8. False-color SEM micrographs of the interaction between *S. epidermidis* (yellow spheres $\approx 0.5\text{--}1\ \mu\text{m}$ in diameter) and the different surfaces. a) F-terminated flat diamond, b) H-terminated flat diamond, c) F-terminated bD, d) H-terminated bD, e) F-terminated bSi, and f) H-terminated bSi.

presented in Figures 1a and 2b, in the SEM micrographs, there are relatively few bacteria adhering to all the surfaces.

Additionally, it was observed that some bacteria seemed to be pierced and others visibly deformed from the cell wall rupturing (Figure 7e,f and 8e,f). This finding is consistent with the live–dead staining results and with the results from the literature on Gram-negative bacteria.^[20] These results suggest that the nanostructured surfaces can also kill some Gram-positive bacteria on contact.

4. Conclusion

In conclusion, fluorinated and hydrogenated diamond-coated surfaces, with and without nanoneedles, were found to have repelling, bactericidal, and biofilm-inhibiting effects on both Gram-positive *S. aureus* and *S. epidermidis* bacterial strains and are promising antimicrobial surfaces. Data show in the initial adhesion that black diamond surfaces repel both Gram-positive bacteria, and on the fluorine-terminated black diamond surfaces the highest killing was achieved. However, all the surfaces were far less effective at preventing bacterial build-up following 24 h biofilm formation. This is believed to be due to the remains (e.g., proteins) of the dead bacteria, which were killed initially by contact with the surface, acting as nutrient sources and a protective layer upon which subsequent bacteria could grow. This suggests that the mechanical killing of bacteria in this way could be improved with frequent washing of the surfaces to remove any bacterial remains and re-expose the underlying bactericidal surface.

Supporting Information

Supporting Information is available from the Wiley Online Library or from the author.

Acknowledgements

N.N. and W.W. contributed equally to this work. The authors wish to thank the European commission for funding via grant no. MagnetoVirology, 838494.

Conflict of Interest

The authors declare no conflict of interest.

Data Availability Statement

The data that support the findings of this study are available from the corresponding author upon reasonable request or from the University of Bristol data repository at <https://doi.org/10.5523/bris.37kjcceqz0f2lvf8zlfynjdp>.

Keywords

bacteria, black diamond, black silicon, diamonds

Received: July 7, 2023
Published online: August 15, 2023

- [1] S. Tian, L. Su, Y. Liu, J. Cao, G. Yang, Y. Ren, F. Huang, J. Liu, Y. An, H. C. van der Mei, H. J. Busscher, L. Shi, *Sci. Adv.* **2020**, *6*, abb1112.
- [2] Y. Liu, H. C. van der Mei, B. Zhao, Y. Zhai, T. Cheng, Y. Li, Z. Zhang, H. J. Busscher, Y. Ren, L. Shi, *Adv. Funct. Mater.* **2017**, *27*, 1701974.
- [3] M. A. Wahab, L. Li, H. Li, A. Abdala, *Nanomaterials* **2021**, *11*, 581.
- [4] S. Gulla, D. Lomada, V. V. S. S. Srikanth, M. V. Shankar, K. R. Reddy, S. Soni, M. C. Reddy, In *Methods in Microbiology*, Vol. 46 (Eds: V. Gurtler, A. S. Ball, S. Soni), Nanotechnology; Academic Press **2019**, p. 255, <https://doi.org/10.1016/bs.mim.2019.03.003>.
- [5] Y. Luan, S. Liu, M. Pihl, H. C. van der Mei, J. Liu, F. Hizal, C.-H. Choi, H. Chen, Y. Ren, H. J. Busscher, *Curr. Opin. Colloid Interface Sci.* **2018**, *38*, 170.
- [6] A. Ziębowicz, A. Sambok-Kielbowicz, W. Walke, A. Mzyk, K. Kosiel, J. Kubacki, B. Bączkowski, M. Pawlyta, B. Ziębowicz, *Materials* **2021**, *14*, 1079.
- [7] X. Ding, S. Duan, X. Ding, R. Liu, F.-J. Xu, *Adv. Funct. Mater.* **2018**, *28*, 1802140.
- [8] W. Li, E. S. Thian, M. Wang, Z. Wang, L. Ren, *Adv. Sci.* **2021**, *8*, 2100368.
- [9] J. Jenkins, M. I. Ishak, M. Eales, A. Gholinia, S. Kulkarni, T. F. Keller, P. W. May, A. H. Nobbs, B. Su, *iScience* **2021**, *24*, 102818.
- [10] S. M. Kelleher, O. Habimana, J. Lawler, B. O' Reilly, S. Daniels, E. Casey, A. Cowley, *ACS Appl. Mater. Interfaces* **2016**, *8*, 14966.
- [11] Y. Liu, L. Shi, L. Su, H. C. van der Mei, P. C. Jutte, Y. Ren, H. J. Busscher, *Chem. Soc. Rev.* **2019**, *48*, 428.
- [12] X. Chen, Z. Wang, J. Wu, *J. Polym. Res.* **2018**, *25*, 48.
- [13] F. Xue, J. Liu, L. Guo, L. Zhang, Q. Li, *J. Theor. Biol.* **2015**, *385*, 1.
- [14] E. P. Ivanova, J. Hasan, H. K. Webb, G. Gervinskas, S. Juodkazis, V. K. Truong, A. H. F. Wu, R. N. Lamb, V. A. Baulin, G. S. Watson, J. A. Watson, D. E. Mainwaring, R. J. Crawford, *Nat. Commun.* **2013**, *4*, 2838.
- [15] J. Oh, H.-C. Yuan, H. M. Branz, *Nat. Nanotech.* **2012**, *7*, 743.
- [16] A. B. Roy, A. Dhar, M. Choudhuri, S. Das, S. M. Hossain, A. Kundu, *Nanotechnology* **2016**, *27*, 305302.
- [17] W. Kim, J. K. Ng, M. E. Kunitake, B. R. Conklin, P. Yang, *J. Am. Chem. Soc.* **2007**, *129*, 7228.
- [18] A. K. Shalek, J. T. Robinson, E. S. Karp, J. S. Lee, D. R. Ahn, M. H. Yoon, A. Sutton, M. Morgolli, R. S. Gertner, T. S. Gujral, G. MacBeath, E. G. Yang, H. Park, *Proc. Natl. Acad. Sci. U. S. A.* **2010**, *107*, 1870.
- [19] D. P. Linklater, H. K. D. Nguyen, C. M. Bhadra, S. Juodkazis, E. P. Ivanova, *Nanotechnology* **2017**, *28*, 245301.
- [20] G. Hazell, P. May, W. P. Taylor, A. H. Nobbs, C. C. Welch, B. Su, *Biomater. Sci.* **2018**, *6*, 1424.
- [21] P. W. May, M. Clegg, T. A. Silva, H. Zanin, O. Fatibello-Filho, V. Celorrio, D. J. Fermin, C. C. Welch, G. Hazell, L. Fisher, A. Nobbs, B. Su, *J. Mater. Chem. B* **2016**, *4*, 5737.
- [22] O. Dunseath, E. J. W. Smith, T. Al-Jeda, J. A. Smith, S. King, P. W. May, A. H. Nobbs, G. Hazell, C. C. Welch, B. Su, *Sci. Rep.* **2019**, *9*, 8815.
- [23] C. Valotteau, I. M. Banat, C. A. Mitchell, H. Lydon, R. Marchant, F. Babonneau, C.-M. Pradier, N. Baccile, V. Humblot, *Colloids Surf. B* **2017**, *157*, 325.
- [24] J. Li, L. Tan, X. Liu, Z. Cui, X. Yang, K. W. K. Yeung, P. K. Chu, S. Wu, *ACS Nano* **2017**, *11*, 11250.
- [25] B. Gottenbos, *J. Antimicrob. Chemother.* **2001**, *48*, 7.
- [26] Z. M. ShalabayevBaláž, M. Baláž, N. Daneu, E. Dutková, Z. Bujňáková, M. Kaňuchová, Z. Danková, Ľ. Balážová, F. Uraekav, Ľ. Tkáčiková, M. Burkitbayev, *ACS Sustainable Chem. Eng.* **2019**, *7*, 12897.

- [27] M. Crismaru, L. A. T. W. Asri, T. J. A. Looijens, B. P. Krom, J. de Vries, H. C. van der Mei, H. J. Busscher, *Antimicrob. Agents Chemother.* **2011**, *55*, 5010.
- [28] M. G. Katsikogianni, Y. F. Missirlis, *Acta Biomater.* **2010**, *6*, 1107.
- [29] T. A. Taylor, C. G. Unakal, In *StatPearls*, StatPearls Publishing, Treasure Island, FL **2022**.
- [30] M. C. Enright, D. A. Robinson, G. Randle, E. J. Feil, H. Grundmann, B. G. Spratt, *Proc. Natl. Acad. Sci.* **2002**, *99*, 7687.
- [31] M. Otto, *Nat. Rev. Microbiol.* **2009**, *7*, 555.
- [32] W. F. Oliveira, P. M. S. Silva, R. C. S. Silva, G. M. M. Silva, G. Machado, L. C. B. B. Coelho, M. T. S. Correia, *J. Hosp. Infect.* **2018**, *98*, 111.
- [33] P. W. May, *Phil. Trans. R. Soc. London, Ser. A* **2000**, *358*, 473.
- [34] N. Norouzi, Y. Ong, V. G. Damle, M. B. Habibi Najafi, R. Schirhagl, *Mater. Sci. Eng. C* **2020**, *112*, 110930.
- [35] J. Schindelin, I. Arganda-Carreras, E. Frise, V. Kaynig, M. Longair, T. Pietzsch, S. Preibisch, C. Rueden, S. Saalfeld, B. Schmid, J.-Y. Tinevez, D. J. White, V. Hartenstein, K. Eliceiri, P. Tomancak, A. Cardona, *Nat. Methods* **2012**, *9*, 676.
- [36] A. Heydorn, A. T. Nielsen, M. Hentzer, C. Sternberg, M. Givskov, B. K. Ersbøll, S. Y. Molin, *Microbiology* **2000**, *146*, 2395.
- [37] M. Vorregaard, *Comstat2 - A Modern 3D Image Analysis Environment for Biofilms*. 85, Technical University of Denmark, Denmark **2008**, <http://www.comstat.dk/> (accessed: July 2023).
- [38] J. Hou, C. Wang, R. T. Rozenbaum, N. Gusnaniar, E. D. de Jong, W. Woudstra, G. I. Geertsema-Doornbusch, J. Atema-Smit, J. Sjollem, Y. Ren, H. J. Busscher, H. C. van der Mei, *Sci. Rep.* **2019**, *9*, 9794.
- [39] M. R. Nejadnik, H. C. van der Mei, W. Norde, H. J. Busscher, *Biomaterials* **2008**, *29*, 4117.
- [40] A. Krasowska, K. Sigler, *Front. Cell. Infect. Microbiol.* **2014**, *4*, 112.
- [41] H.-Y. Wang, X.-W. Hua, F.-G. Wu, B. Li, P. Liu, N. Gu, Z. Wang, Z. Chen, *ACS Appl. Mater. Interfaces* **2015**, *7*, 7082.
- [42] J. Jenkins, J. Mantell, C. Neal, A. Gholinia, P. Verkade, A. H. Nobbs, B. Su, *Nat. Commun.* **2020**, *11*, 1626.
- [43] S. R. Hemelaar, B. Saspaanithy, S. R. M. L'Hommelet, F. P. Perona Martinez, K. J. Van der Laan, R. Schirhagl, *Sensors* **2018**, *18*, 355.
- [44] N. Norouzi, A. C. Nusantara, Y. Ong, T. Hamoh, L. Nie, A. Morita, Y. Zhang, A. Mzyk, R. Schirhagl, *Carbon* **2022**, *199*, 444.
- [45] A. Mai-Prochnow, M. Clauson, J. Hong, A. B. Murphy, *Sci. Rep.* **2016**, *6*, 38610.
- [46] X. Li, K.-H. Tsui, J. K. H. D. W. TsoiGreen, D. W. Green, X. Jin, Y. Qiang Deng, Y. Min Zhu, X. Guang Li, Z. Fan, G. Shun-pan Cheung, *Nanoscale* **2020**, *12*, 18864.
- [47] T. T. Gupta, N. K. Gupta, M. J. Pestrak, D. H. Dusane, J. M. Harro, A. R. Horswill, P. Stoodley, *Appl. Environ. Microbiol.* **2020**, *86*, e01234.
- [48] S. N. L. Talluri, R. M. Winter, D. R. Salem, *Biofouling* **2020**, *36*, 183.
- [49] H. Boudarel, J.-D. Mathias, B. Blaysat, M. Grédiac, *npj Biofilms Microbiomes* **2018**, *4*, 1.
- [50] H.-C. Flemming, J. Wingender, *Nat. Rev. Microbiol.* **2010**, *8*, 623.
- [51] R. T. Pena, L. Blasco, A. Ambroa, B. González-Pedrajo, L. Fernández-García, M. López, I. Blieriot, G. Bou, R. García-Contreras, T. K. Wood, M. Tomás, *Front. Microbiol.* **2019**, *10*, 1100.